CHAPTER 5

BEARINGS WITH AXIAL CURRENT

In chapter three we saw that significant increases in load capacity of bearings could be effected by the application of magnetic fields. In this chapter we study the effect of axial current induced pinch on bearings.

In the first of the following sections we study the effects of axial current induced pinch on the squeeze film behaviour between (i) two annular disks (ii) two circular disks, the non-rotating upper disk having a porous facing and the non-porous lower disk rotating. Rotating porous circular disks with no axial current are discussed as a special case. In the other section we study the axial pinch effect on the curved squeeze film between two circular plates.

5.1 ROTATING POROUS ANNULAR AND CIRCULAR DISKS

Elco and Hughes [26] initiated the study of axial current induced pinch effect on non-porous bearings and many others followed. Gupta and Sinha [27] initiated such study on porous bearings by considering porous annular disks. They showed that the film pressure, the load capacity

and the time of approach increased due to the pinch. Moreover, an amount of load could be sustained by the bearing even when there was no flow. Gupta and Patel [28] extended the analysis [27] by including the effect of velocity slip at the porous boundary. Later, Hingu [29] considered the effect of axial current induced pinch on porous circular disks.

Wu [23] analysed the squeeze film behaviour between rotating porous annular disks. He showed that the effect of rotation was to reduce pressure, load capacity and response time. The criteria under which the inertia effects could be neglected were also given. Prakash and Vij [54] extended the analysis of Wu [23] to include the effect of velocity slip at the porous boundary. They showed that the effect of velocity slip was to reduce the load capacity and the response time further.

All the above studies on porous bearings gave the results in terms of the Fourier-Bessel series. Patel [30] simplified the analysis of axial pinch effects on non-rotating porous annular and circular plates by using Morgan-Cameron approximation. Ting [24] presented

the analysis for the case of squeeze film behaviour between porous annular disks with the non-porous disk rotating and the non-rotating porous disk approaching the first one normally. He utilised simplifying assumptions to obtain the solutions which are quite easy for computational purposes.

Here we apply the method of Ting [24] to determine the effects of axial current induced pinch on rotating porous annular as well as circular disks.

The flow is axisymmetric. The induced magnetic fields in the axial and radial directions are negligible. The radial velocity components of the fluid in the film and the porous regions are so small that induced axial electric fields can be neglected. It is assumed that all the inertia terms except the centrifugal force term can be neglected.

5.1.1 Mathematical formulation

Each of the bearing configurations consists of a non-rotating upper disk which has a porous facing of thickness H and which moves normally towards the parallel lower disk which is non-porous and rotates at an angular velocity Ω (Figs. 12 and 13).

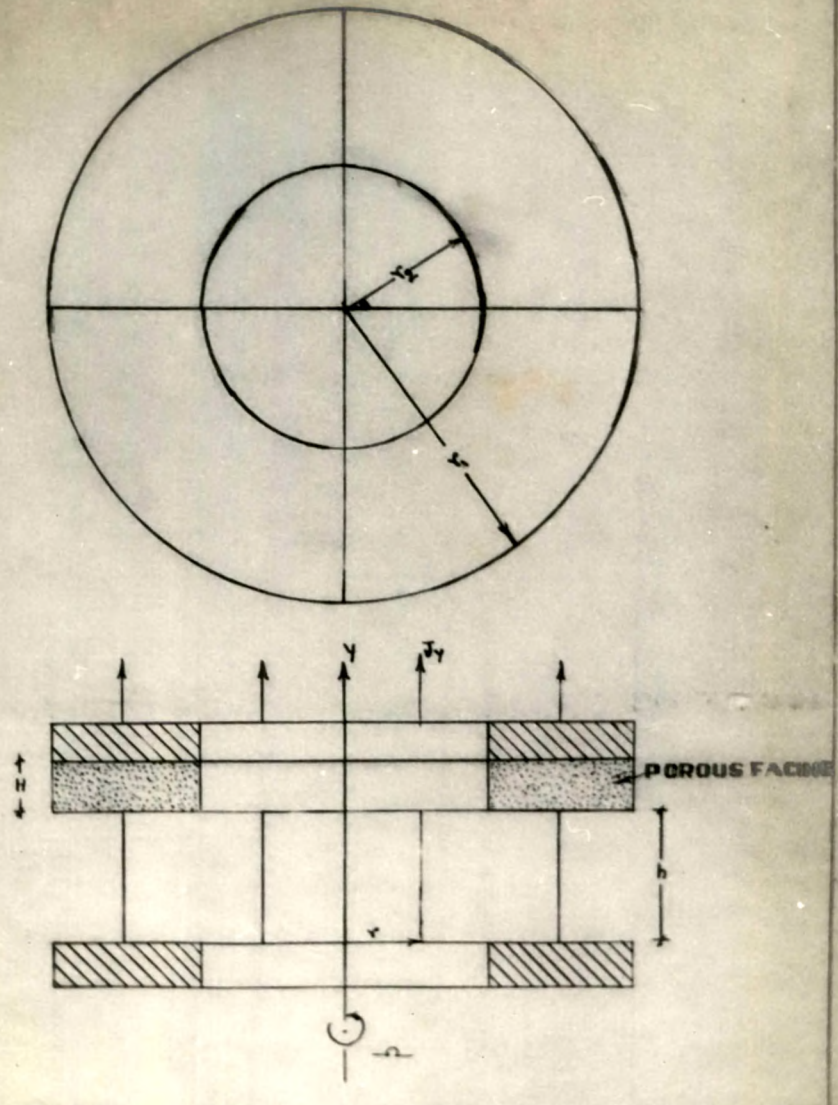

FIG. 12. ROTATING POROUS ANNULAR DISCS.

Application of a potential between the conducting disks produces an axial current density J_y between them. J_y gives rise to an azimuthal magnetic induction B_θ. Interaction of J_y and B_θ provides a radial body force proportional to $J_y B_\theta$ which results in the pinch effect that can increase the load capacity of the system.

In the present case the equations governing the flows in the two regions take the following forms :

Film region :

$$J_y B_\theta - \rho \frac{w^2}{r} = - \frac{\partial p}{\partial r} + \mu \frac{\partial^2 u}{\partial y^2} \tag{1}$$

$$0 = \mu \frac{\partial^2 w}{\partial y^2} \tag{2}$$

$$0 = - \frac{\partial p}{\partial y} + \mu \frac{\partial^2 v}{\partial y^2} \tag{3}$$

$$\frac{1}{r} \frac{\partial}{\partial r} (ru) + \frac{\partial v}{\partial y} = 0 \tag{4}$$

Porous region :

$$V_r = - \frac{k}{\mu} \left[\frac{\partial P}{\partial r} + J_y B_\theta \right] \tag{5}$$

$$V_y = -\frac{k}{\mu} \frac{\partial P}{\partial y} \tag{6}$$

$$\frac{1}{r} \frac{\partial}{\partial r} (r V_r) + \frac{\partial V_y}{\partial y} = 0, \tag{7}$$

where u, v and V_r, V_y are the radial and axial components of the fluid velocities in the film and the porous regions respectively, and w is the tangential component of the fluid velocity in the film region.

Equation (2) can be integrated with the boundary conditions

$w = r\Omega$ when $y = 0$ and $w = 0$ when $y = h$

to obtain

$$w = r\Omega \left(1 - \frac{y}{h}\right), \tag{8}$$

Integrating equation (3) twice with respect to y, we obtain

$$\int p \, dy = \mu v + C_1 y + C_2 , \tag{9}$$

where C_1 and C_2 are functions of r only.

Using the boundary conditions

$$v_0 = 0 \quad \text{and} \quad v_h = \frac{dh}{dt} - \frac{k}{\mu}\left(\frac{\partial P}{\partial y}\right)_{y=h} \tag{10}$$

in equation (9), we obtain

$$C_2 = 0 \quad \text{and} \quad C_1 = \frac{1}{h}\int_0^h p\, dy - \frac{\mu}{h}\left[\frac{dh}{dt} - \frac{k}{\mu}\left(\frac{\partial P}{\partial y}\right)_{y=h}\right]. \tag{11}$$

From Maxwell's equations and the Ohm's law, it can be shown that [27]

$$B_\theta = \frac{1}{2}\mu_e J_y r. \tag{12}$$

The total current I is defined as

$$I = \int_{r_2}^{r_1} 2\pi r J_y\, dr,$$

where $r_2 = 0$ in the case of circular disks, so that

$$J_y = \frac{I}{\pi (r_1^2 - r_2^2)}. \tag{13}$$

From equations (12) and (13) we find

$$J_y B_\theta = c^* r, \tag{14}$$

where

$$c^* = \frac{\mu_e I^2}{2\pi^2 (r_1^2 - r_2^2)^2} \tag{15}$$

From equations (5) - (7), we have

$$\frac{1}{r} \frac{\partial}{\partial r} \left(r \frac{\partial P}{\partial r} + c^* r^2 \right) + \frac{\partial^2 P}{\partial y^2} = 0, \tag{16}$$

using (14).

Averaging P over the thickness H of the porous facing and using

$$\left(\frac{\partial P}{\partial y} \right)_{y = h+H} = 0,$$

equation (16) yields

$$\left(\frac{\partial P}{\partial y} \right)_{y=h} = \frac{H}{r} \frac{\partial}{\partial r} \left(r \frac{\partial P}{\partial r}^* + c^* r^2 \right), \tag{17}$$

where

$$P^* = \frac{1}{H} \int_h^{h+H} P \, dy.$$

Using equations (11) and (17) in (9) and then differentiating it once with respect to y, we obtain

$$p = \mu \frac{\partial v}{\partial y} + p^* - \frac{\mu}{h} \frac{dh}{dt} + \frac{kH}{h} \frac{1}{r} \frac{\partial}{\partial r} \left(r \frac{\partial P^*}{\partial r} + c^* r^2 \right), \qquad (18)$$

where

$$p^* = \frac{1}{h} \int_0^h p \, dy.$$

Introducing equations (8), (14) and (18) in (1), we have

$$\frac{\partial p^*}{\partial r} + c^* r - r\rho\Omega^2 \left(1 - \frac{y}{h}\right)^2 + \mu \frac{\partial}{\partial r} \left(\frac{\partial v}{\partial y} \right)$$

$$+ \frac{kH}{h} \frac{\partial}{\partial r} \left[\frac{1}{r} \frac{\partial}{\partial r} \left(r \frac{\partial P^*}{\partial r} + c^* r^2 \right) \right] = \mu \frac{\partial^2 u}{\partial y^2}. \qquad (19)$$

Using equation (4) in (19) and rearranging, we obtain

$$\frac{\partial p^*}{\partial r} + c^* r + \frac{kH}{h} \frac{\partial}{\partial r} \left[\frac{1}{r} \frac{\partial}{\partial r} \left(r \frac{\partial P^*}{\partial r} + c^* r^2 \right) \right]$$

$$= \mu \left[\frac{\partial^2 u}{dy^2} + \frac{\partial}{\partial r} \left\{ \frac{1}{r} \frac{\partial}{\partial r} (ru) \right\} \right] + \rho r \Omega^2 \left(1 - \frac{y}{h}\right)^2. \qquad (20)$$

Using the dimensionless quantities defined below

$$r = r'r_1,\ y = y'h_0\ ,\ u = u'U,\ p^* = p^{*'}p_0\ ,$$

$$P^* = P^{*'}p_0\ ,\quad h = h'h_0$$

and assuming that h_0 is very small compared to r_1 so that quadratic terms of $\frac{h_0}{r_1}$ may be neglected as in [24] , equation (20) reduces to

$$\frac{\partial p^{*'}}{\partial r'} + \frac{c^* r_1^2 r'}{p_0} = \frac{\mu U r_1}{p_0 h_0^2}\ \frac{\partial^2 u'}{\partial y'^2} + \frac{\rho r_1^2 \Omega^2 r'}{p_0}\left(1 - \frac{y'}{h'}\right)^2.$$

Reverting back to the dimensional variables, it takes the form

$$\frac{\partial p^*}{\partial r} + c^* r = \mu \frac{\partial^2 u}{\partial y^2} + \rho r \Omega^2 \left(1 - \frac{y}{h}\right)^2. \qquad (21)$$

Solving equation (21) under the no-slip boundary conditions on both the surfaces, we obtain

$$u = -\frac{1}{2\mu}\left(\frac{\partial p^*}{\partial r} + c^* r\right) y(h - y)$$

$$+ \frac{h^3}{12\mu} \rho \Omega^2 r \left[\left(1 - \frac{y}{h}\right) - \left(1 - \frac{y}{h}\right)^4\right]. \qquad (22)$$

Integrating equation (4) with respect to y across the film, using the condition $v_o = 0$ and then substituting (22) in it, we have

$$\frac{1}{r}\frac{d}{dr}\left(r\frac{dp^*}{dr} + c^* r^2\right) = \frac{3}{5}\rho\Omega^2$$

$$+ \frac{12\mu}{h^3}\left[\dot{h} - \frac{kH}{\mu}\frac{1}{r}\frac{d}{dr}\left(r\frac{dP^*}{dr} + c^* r^2\right)\right]. \qquad (23)$$

Assuming that the mean pressure p^* in the film region and the mean pressure P^* in the porous region are equal at any r for small values of H/r_1, equation (23) may be written as

$$\frac{1}{r}\frac{d}{dr}\left[r\frac{d}{dr}\left\{\left(1 + 12\frac{kH}{h^3}\right)p^*\right\}\right]$$

$$= \frac{3}{5}\rho\Omega^2 + 12\mu\frac{\dot{h}}{h^3} - 2c^*\left(1 + 12\frac{kH}{h^3}\right) \qquad (24)$$

5.1.2 Solutions for rotating porous annular disks

Solving equation (24) with the boundary conditions $p(r_1) = p(r_2) = 0$, gives the pressure distribution as

$$\frac{h^3 p^*}{\mu r_2^2 \dot{h}} = 3 \left[\frac{1 + 4\frac{S}{\sigma^*}}{1 + 12\psi^*} - \frac{c^* h^3}{6\mu \dot{h}} \right] \left(\frac{r_1^2}{r_2^2} - 1 \right) \left[\frac{r^2 - r_2^2}{r_1^2 - r_2^2} - \frac{\ln\left(\frac{r}{r_2}\right)}{\ln\left(\frac{r_1}{r_2}\right)} \right] . \qquad (25)$$

The load carrying capacity is

$$\frac{h^3 W}{\mu r_2^4 \dot{h}} = -\frac{3\pi}{2} \left[\frac{1 + 4\frac{S}{\sigma^*}}{1 + 12\psi^*} - \frac{c^* h^3}{6\mu \dot{h}} \right] D \qquad (26)$$

and the time taken to reach a film thickness from h_0 to h_1 is

$$\Delta t = \int_{t_0}^{t_1} dt = -\frac{3\pi}{2} \frac{\mu\, r_2^4\, D}{\left(W - \frac{\pi}{4} c^*\, r_2^4\, D\right) h_0^2}$$

$$\cdot \frac{1}{\left[1 + \frac{3}{40} \frac{\pi \rho \Omega^2 r_2^4 D}{W - \frac{\pi}{4} c^* r_2^4 D}\right]} \int_1^{\bar{h}_1} \frac{d\bar{h}}{\bar{h}^3 + k^{*3}}$$

$$= -\frac{3\pi}{2} \frac{\mu\, r_2^4\, D}{\left(W - \frac{\pi}{4} c^* r_2^4 D\right) h_0^2 \left[1 + \frac{3}{40} \frac{\pi \rho \Omega^2 r_2^4 D}{W - \frac{\pi}{4} c^* r_2^4 D}\right]}$$

$$\cdot \frac{1}{3k^{*2}} \left[\frac{1}{2} \ln \frac{(k^* + \bar{h}_1)^2 (k^{*2} - k^* + 1)}{(k^* + 1)^2 (k^{*2} - k^* \bar{h}_1 + \bar{h}_1^2)} \right.$$

$$\left. + \sqrt{3} \left\{ \tan^{-1} \left(\frac{2\bar{h}_1 - k^*}{k^* \sqrt{3}} \right) - \tan^{-1} \left(\frac{2 - k^*}{k^* \sqrt{3}} \right) \right\} \right] \qquad (27)$$

where

$$\left.\begin{aligned} &\bar{h} = \frac{h}{h_0}\ ,\quad \bar{h}_1 = \frac{h_1}{h_0}\ ,\quad D = \frac{r_1^4}{r_2^4} - 1 - \frac{\left(\frac{r_1^2}{r_2^2} - 1\right)^2}{\ln\left(\frac{r_1}{r_2}\right)} \\ &\psi^* = \frac{kH}{h^3} = \psi_0 \left(\frac{h_0}{h}\right)^3\ ,\quad S = \frac{3}{20}\ \frac{\rho\Omega^2 r_2^2}{p_0}\ , \\ &\sigma^* = \frac{12\ r_2^2\ \mu\dot{h}}{p_0\ h^3}\ ,\quad k^* = \left[\ \frac{12\ \psi_0}{1 + \frac{3}{40}\ \frac{\pi\rho\Omega^2 r_2^4\ D}{\left(W - \frac{\pi}{4}\ c^* r_2^4\ D\right)}}\ \right]^{1/3}. \end{aligned}\right\} \quad (28)$$

By making the current parameter $c^* = 0$, equations (25) - (27) agree with those obtained by Ting [24].

5.1.3 Results and discussion

From equations (25) and (26), it may be observed that the pressure distribution in the film region and the load capacity are increased due to the pinch effect

by quantities

$$\frac{c^*}{2}\left[\, r_2^2 - r^2 + (r_1^2 - r_2^2)\,\frac{\ln\left(\frac{r}{r_2}\right)}{\ln\left(\frac{r_1}{r_2}\right)}\,\right] \tag{29}$$

and

$$\frac{c^*\pi}{4}\left[\, r_1^4 - r_2^4 - \frac{(r_1^2 - r_2^2)^2}{\ln\left(\frac{r_1}{r_2}\right)}\,\right] \tag{30}$$

respectively.

Equation (27) shows that the time of approach in this case is equivalent to that in the corresponding non-magnetic case carrying the load

$$W = \frac{\pi}{4}\, c^*\, r_2^4\, D. \tag{31}$$

Quantities (29) - (31) are the same as those obtained by Gupta and Sinha [27]. Equation (26) also shows that a load equal to $\frac{\pi}{4}\, c^*\, r_2^4\, D$ is supported by the bearing even when there is no flow. There is no interaction between the fluid inertia and the axial current induced pinch effect.

5.1.4 Solutions for rotating porous circular disks

Results for the case of circular disks can not be obtained from the solutions for annular disks because there is a logarithmic singularity at the origin as can be seen from equation (25). Hence we try to construct the solution of equation (24) separately in the present case.

Take the radius of each of the disks to be r_1 and the current parameter to be c_1^*. Then, by setting $r_2 = 0$ in equation (15), we obtain

$$c_1^* = \frac{\mu_e I^2}{2\pi^2 r_1^4} .$$

Solving equation (24) under the boundary conditions

$$p^*(r_1) = 0 \quad \text{and} \quad p^*(0) = \text{finite} ,$$

the pressure distribution is

$$\frac{h^3 p^*}{\mu r_1^2 \dot{h}} = -3 \left[\frac{1 + 4 \frac{S_1}{\sigma_1}}{1 + 12 \psi^*} - \frac{c_1^* h^3}{6 \mu \dot{h}} \right] \left(1 - \frac{r^2}{r_1^2}\right). \qquad (32)$$

The load carrying capacity is

$$\frac{h^3 W}{\mu r_1^4 \dot{h}} = -\frac{3\pi}{2}\left[\frac{1+4\frac{S_1}{\sigma_1}}{1+12\psi^*} - \frac{c_1^* h^3}{6\mu \dot{h}}\right]. \qquad (33)$$

The time taken to reach a film thickness from h_0 to h_1 is given by

$$\Delta t = -\frac{3\pi}{2}\frac{\mu r_1^4}{(W-\frac{\pi}{4}c_1^* r_1^4)h_0^2\left[1+\frac{3}{40}\frac{\pi\rho\Omega^2 r_1^4}{(W-\frac{\pi}{4}c_1^* r_1^4)}\right]}$$

$$\cdot\ \frac{1}{3k_1^{*2}}\left[\frac{1}{2}\ln\frac{(k_1^*+\bar{h}_1)^2(k_1^{*2}-k_1^*+1)}{(k_1^*+1)^2(k_1^{*2}-k_1^*\bar{h}_1+\bar{h}_1^2)}\right.$$

$$\left. +\sqrt{3}\left\{\tan^{-1}\left(\frac{2\bar{h}_1-k_1^*}{k_1^*\sqrt{3}}\right)-\tan^{-1}\left(\frac{2-k_1^*}{k_1^*\sqrt{3}}\right)\right\}\right], \qquad (34)$$

where

$$S_1 = \frac{3}{20}\,\frac{\rho\Omega^2 r_1^2}{p_0}, \quad \sigma_1 = \frac{12\, r_1^2\, \mu\, \dot{h}}{p_0\, h^3}$$

and

$$k_1^* = \left[\frac{12\,\psi_0}{1 + \frac{3}{40}\,\frac{\pi\rho\Omega^2 r_1^4}{(W - \frac{\pi}{4} c_1^* r_1^4)}}\right]^{1/3}. \qquad (35)$$

Special case

In the special case when $c_1^* = 0$, the corresponding results in dimensionless form, for rotating porous circular disks are

$$\bar{p} = -\frac{h^3 p^*}{\mu r_1^2 \dot{h}} = 3\left[\frac{1 + 4\frac{S_1}{\sigma_1}}{1 + 12\psi^*}\right]\left(1 - \frac{r^2}{r_1^2}\right) \qquad (36)$$

$$\bar{W} = -\frac{h^3 W}{\mu r_1^4 \dot{h}} = \frac{3\pi}{2}\left[\frac{1 + 4\frac{S_1}{\sigma_1}}{1 + 12\psi^*}\right] \qquad (37)$$

and

$$\Delta T = \frac{h_0^2 W}{\mu r_1^4} \Delta t = -\frac{3\pi}{2} \frac{1}{1 + \frac{3}{40} \frac{\pi \rho \Omega^2 r_1^4}{W}}$$

$$\cdot \frac{1}{3k_2^{*2}} \left[\frac{1}{2} \ln \frac{(k_2^* + \bar{h}_1)^2 (k_2^{*2} - k_2^* + 1)}{(k_2^* + 1)^2 (k_2^{*2} - k_2^* \bar{h}_1 + \bar{h}_1^2)} \right.$$

$$\left. + \sqrt{3} \left\{ \tan^{-1} \left(\frac{2\bar{h}_1 - k_2^*}{k_2^* \sqrt{3}} \right) - \tan^{-1} \left(\frac{2 - k_2^*}{k_2^* \sqrt{3}} \right) \right\} \right], \quad (38)$$

where

$$k_2^* = \left[\frac{12 \psi_0}{1 + \frac{3}{40} \frac{\pi \rho \Omega^2 r_1^4}{W}} \right]^{1/3} \quad (39)$$

5.1.5 Results and discussion

Equations (32) and (33) show that the

pressure distribution and load capacity are increased due to the pinch effect by quantities

$\frac{c_1^*}{2}(r_1^2 - r^2)$ and $\frac{\pi}{4} c_1^* r_1^4$ respectively.

The time of approach in the present case is equivalent to the corresponding non-magnetic case with the load

$$W - \frac{\pi}{4} c_1^* r_1^4 .$$

The bearing can support a load

$$\frac{\pi}{4} c_1^* r_1^4$$

even when there is no flow. Moreover, there is no interaction between the fluid inertia and the axial current induced pinch effect.

Special case

Equations (36) and (37) give the pressure distribution and the load capacity for porous circular disks, in the non-magnetic case, taking rotating

fluid inertia into consideration, while equation (38) gives the squeeze time in terms of the film thickness. These results are shown graphically in Figures 14 to 17.

Fig. 14 shows the dimensionless mean squeeze film pressure distribution as a function of $\frac{r}{r_1}$ and $\frac{S_1}{\sigma_1}$. For a fixed r the pressure increases with increase in $\frac{S_1}{\sigma_1}$.

Fig. 15 shows the pressure as a function of the permeability parameter ψ^* and the inertia parameter $\frac{S_1}{\sigma_1}$. For $\psi^* \leq 0.001$ the pressure is same for a given value of $\frac{S_1}{\sigma_1}$. For $\psi^* > 0.001$ it decreases rapidly. Figures 14 and 15 show that increase in the fluid inertia paramter increases the fluid pressure.

From Fig. 16 the load capacity can be considerably increased by taking very small values of ψ^* and sufficiently large values of $\frac{S_1}{\sigma_1}$.

The time of approach can be increased by decreasing the velocity of rotation of the lower disk

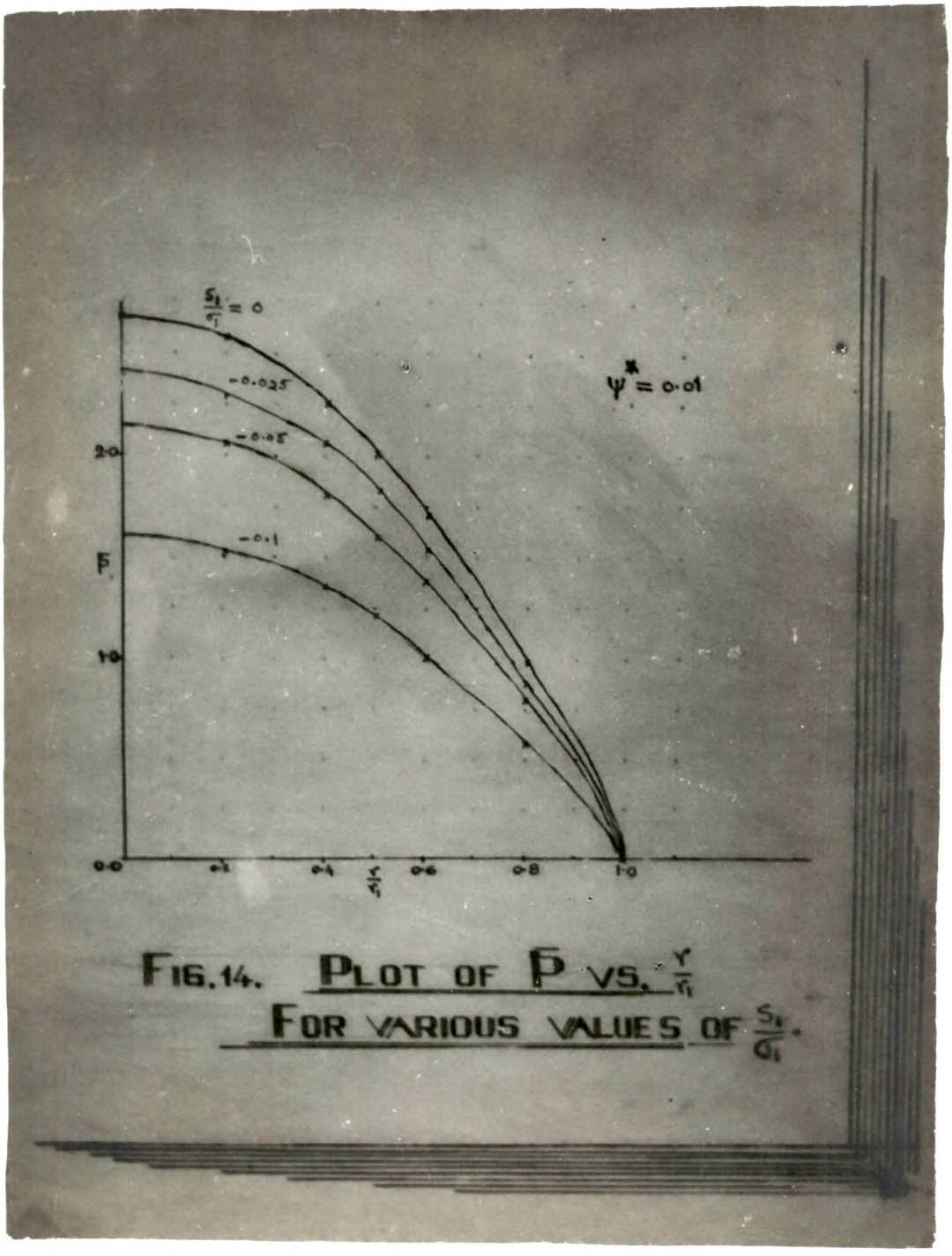

FIG. 14. PLOT OF $\bar{P}$ VS. $\frac{r}{r_1}$ FOR VARIOUS VALUES OF $\frac{S_1}{\sigma_1}$.

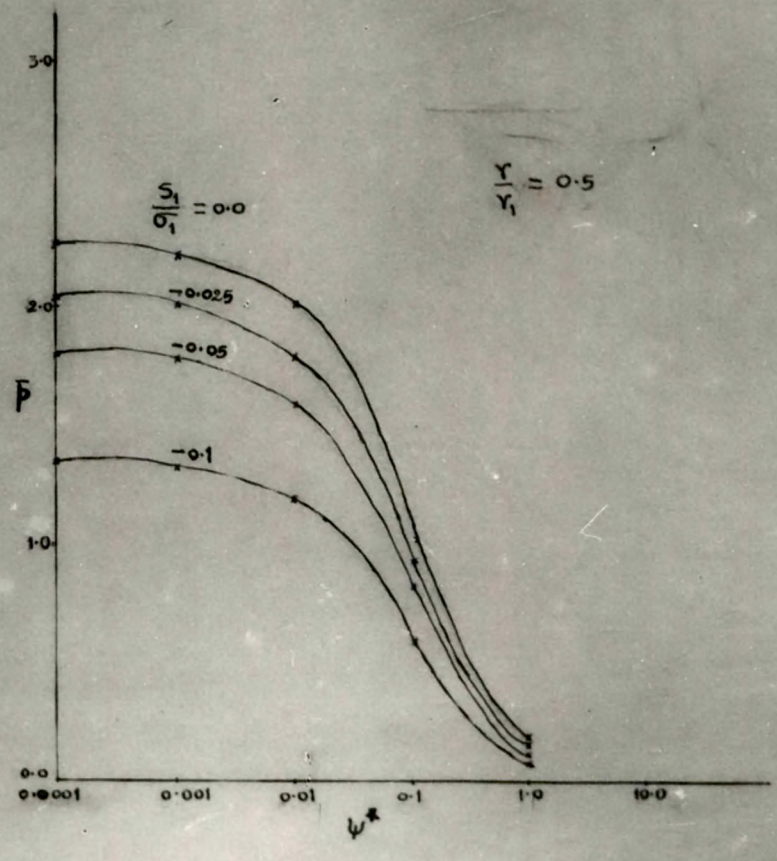

FIG. 15. PLOT OF $\bar{P}$ VS. ψ^* FOR VARIOUS VALUES OF $\frac{S_1}{\sigma_1}$.

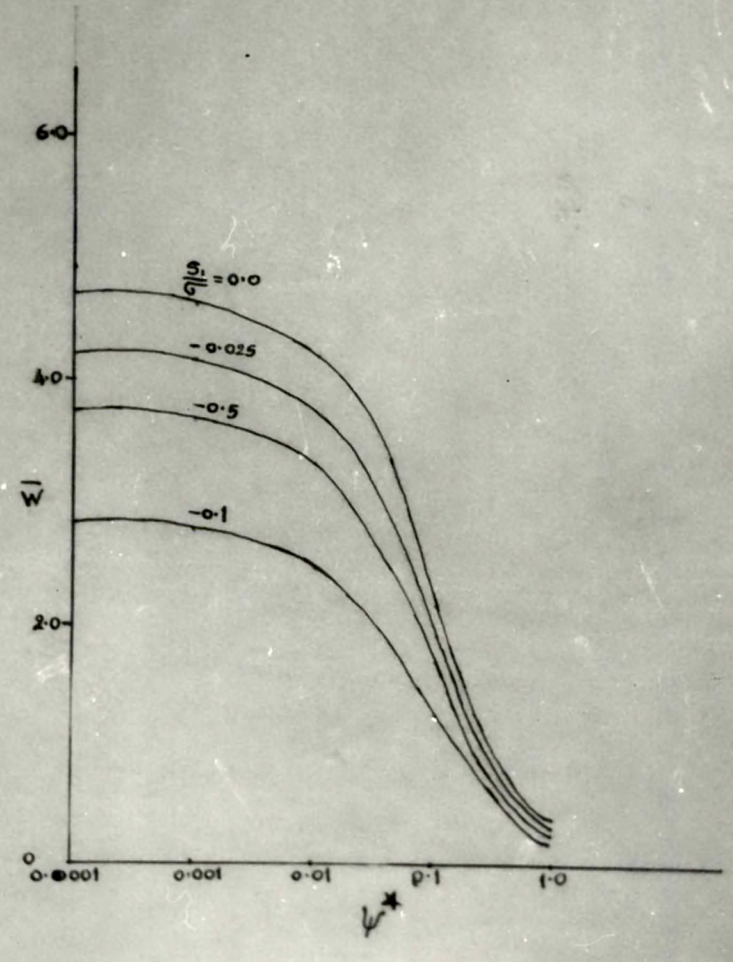

FIG. 16 PLOT OF $\bar{W}$ VS. ψ^* FOR VARIOUS VALUES OF $\frac{S_1}{G_1}$.

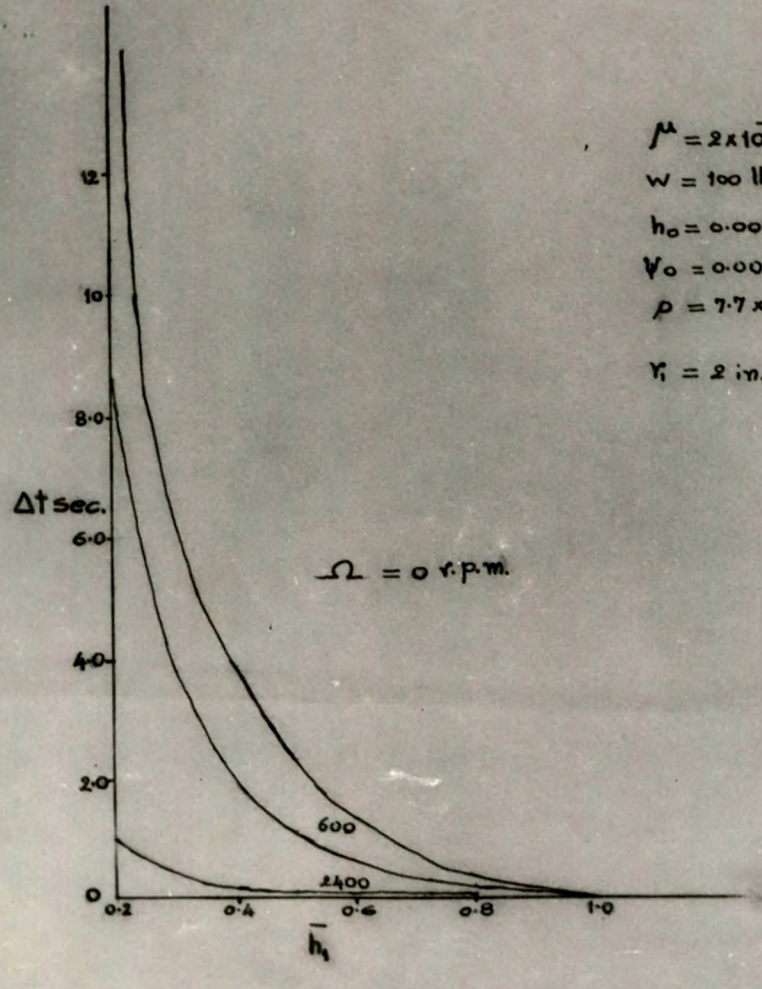

FIG. 17. PLOT OF Δt VS. $\bar{h}_1$ FOR VARIOUS VALUES OF Ω.

is seen from Fig. 17.

Thus the fluid inertia considerably affects the squeeze film behaviour of porous rotating circular disks.

5.2 SQUEEZE FILM BETWEEN CURVED CIRCULAR PLATES

Hays [55] analysed the behaviour of curved squeeze film between non-porous plates, one of which was curved and the other flat. The film shape was taken to be of sine form for both convex and concave pads and the minimum film thickness was maintained as constant. Recently, Murti [43] introduced a new exponential function to describe the film trapped between a curved plate approaching a flat plate by maintaining the central film thickness as constant. He observed that the dimensionless load capacity decreased with increasing curvature parameter $\bar{\beta}$. in the case of convex pads whereas the effect was opposite in the case of concave plates, and, in fact, it sharply rose after a particular $\bar{\beta}$ in the case of concave pads.

In this section, we study the axial current induced pinch effect on the configuration proposed by

Murti [43].

5.2.1 Mathematical formulation

The configuration consists of two plates, each of radius r_1. The upper plate is curved. The lower plate is fixed and flat. The film thickness, as in 2.3.1, is taken as

$$h = \alpha_0 e^{-\beta r^2} , \qquad (40)$$

where α_0 is the central film thickness and β is the curvature of the upper plate.

The upper plate moves normal to itself approaching the lower plate with uniform velocity $\dot{\alpha}_0$. An axial current J_y is applied across the plates which are assumed to be ideal conductors (Fig. 18). This axial current gives rise to an azimuthal magnetic induction B_θ.

With the usual assumptions, the governing equations are

$$\frac{\partial^2 u}{\partial y^2} = \frac{1}{\mu} \left(\frac{dp}{dr} + J_y B_\theta \right) \qquad (41)$$

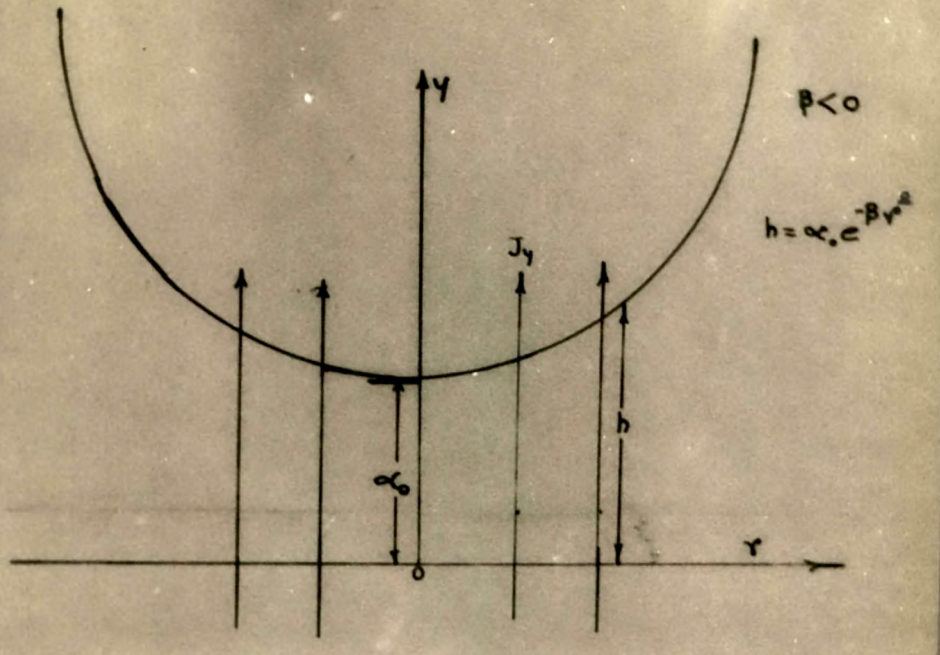

FIG.18. SQUEEZE FILM BETWEEN CURVED CIRCULAR PLATES.

$$\frac{1}{r}\frac{\partial}{\partial r}(ru) + \frac{\partial v}{\partial y} = 0 \qquad (42)$$

From Maxwell's equations and the Ohm's law, it can be shown that [27]

$$B_\theta = \frac{1}{2}\mu_e J_y r, \qquad (43)$$

and

$$J_y = \frac{I}{\pi r_1^2}, \qquad (44)$$

where I is the total current.

From equations (43) and (44), we obtain

$$J_y B_\theta = c_1^* r, \qquad (45)$$

where

$$c_1^* = \frac{\mu_e I^2}{2\pi^2 r_1^4}. \qquad (46)$$

Substituting equation (45) into equation (41), we have

$$\frac{\partial^2 u}{\partial y^2} = \frac{1}{\mu}\left(\frac{dp}{dr} + c_1^* r\right). \qquad (47)$$

Solving equation (47) for u with the boundary conditions

$$u = 0 \quad \text{when} \quad y = 0, h,$$

we have

$$u = \frac{1}{2\mu} \left(\frac{dp}{dr} + c_1^* r \right) y(y-h). \tag{48}$$

Equation (42) may be written in the form

$$\int_0^h \frac{1}{r} \frac{\partial}{\partial r} (ru)\, dy + v_h = 0, \tag{49}$$

since the lower plate is fixed .

Since

$$v_h = \dot{\alpha}_0 , \tag{50}$$

equation (49) takes the form

$$\int_0^h \frac{1}{r} \frac{\partial}{\partial r} (ru)\, dy + \dot{\alpha}_0 = 0 \tag{51}$$

Substituting (48) into equation (51), we have

$$\frac{1}{r} \frac{d}{dr} \left[\left(r \frac{dp}{dr} + c_1^* r^2 \right) h^3 \right] = 12 \mu \dot{\alpha}_0 \tag{52}$$

5.2.2 Solutions

Solving equation (52) under the boundary conditions

$$\frac{dp}{dr} = 0 \quad \text{when} \quad r = 0 \quad \text{and} \quad p = 0 \quad \text{when} \quad r = r_1, \tag{53}$$

the pressure distribution is given by

$$-\frac{\alpha_0^3 p}{\mu r_1^2 \dot{\alpha}_0} = -\frac{c_1^* \alpha_0^3}{2 \mu r_1^2 \dot{\alpha}_0}(r_1^2 - r^2) - \frac{e^{3\beta r^2} - e^{3\beta r_1^2}}{\beta r_1^2}. \tag{54}$$

The load capacity is given by

$$\frac{\alpha_0^3 W}{2\pi \mu |\dot{\alpha}_0| r_1^4} = -\frac{c_1^* \alpha_0^3}{8 \mu \dot{\alpha}_0} - \frac{e^{3\beta r_1^2}(1-3\beta r_1^2) - 1}{6\beta^2 r_1^4} \tag{55}$$

The time for a reduction in film thickness from α_{01} to α_{02} is

$$\Delta t = \frac{2\pi\mu}{\left(W - \frac{\pi}{4} c_1^* r_1^4\right)} \left[\frac{1}{2} \left(\frac{1}{\alpha_{02}^2} - \frac{1}{\alpha_{01}^2} \right) \right] \cdot \frac{1 - (1 - 3\beta r_1^2) e^{3\beta r_1^2}}{6\beta^2} . \qquad (56)$$

5.2.3 Results and discussion

When $c_1^* = 0$, equations (54) - (56) agree with the hydrodynamic case of Murti [43].

Equations (54) and (55) show that the pressure and the load capacity are substantially increased due to the pinch effect by the quantities

$$\frac{c_1^*}{2} (r_1^2 - r^2) \quad \text{and} \quad \frac{\pi}{4} c_1^* r_1^4 \quad \text{respectively.}$$

Equation (56) shows that the time of approach is increased by the pinch effect and that it is equivalent to the corresponding non-magnetic case with an equivalent load $W - \frac{\pi}{4} c_1^* r_1^4$. From

equation (55), when there is no flow, a load equal to $\frac{\pi}{4} c_1^* r_1^4$ is sustained by the bearing. Increases in pressure, load capacity and time of approach are the same as those of exact analysis of Hingu [29] and of the approximate analysis of Patel [30] on the porous squeeze film between parallel flat plates. As they are independent of β, these increases do not depend on the concavity or the convexity of the pad.

REFERENCES

1. Cameron, A. — Principles of lubrication. Longmanns (1966).

2 DeWiest, R.J.M. — Flow through porous media. Academic Press (1969).

3 Booser, E.R. — Bearing materials and properties. Machine Design, 38 (6) 22-28 (1966).

4 Saibel, E.A., and Macken, N. A. — The fluid mechanics of lubrication. Annual Review of Fluid Mechanics, 5 185-212 (1973).

5 Sinha, P.C., and Gupta, J.L. — Hydromagnetic squeeze films between porous rectangular plates. Trans. ASME, F 95 394-398 (1973).

6 Cusano, C. — Lubrication of a two-layer porous journal bearing. J. Mech. Engng. Sci., 14 , 335-339 (1972).

7 Heller, S., Shapiro, W., and Decker, O. — A porous hydrostatic gas bearing for use in a miniature turbomachinery. Trans. ASLE, 14 , 144-155 (1971).

8 Sneck, H. J. — A survey of gas lubricated porous bearings Trans. ASME, F 90 804-809 (1968).

9 Morgan, V.T., and Cameron, A. — Mechanism of lubrication in porous metal bearings. Proc. of the Conf. on Lubrication and Wear, Inst. Mech. Engrs., London, paper 89 151-157 (1957).

10 Prakash, J., and Vij, S.K. — Load capacity and time-height relations for squeeze films between porous plates. Wear, 24 309-322 (1973).

11 Ene, H. I. — Sur le probleme de Hartmann pour le movement d'un fluide electroconducteur dans un millieu poreuse homogene. C.R. Acad. Sci. Paris, A.B. 268 564-565 (1969).

12 Hughes, W.F., and Elco, R.A. — Magnetohydrodynamic lubrication between parallel rotating disks. J. Fluid. Mech., 13 21-32 (1962).

13 Kulkarni, S.V., and Vinay Kumar. — Lubrication equation for non-isotropic porous bearings considering slip velocity. J. Inst. Engrs., India, 56 Part ME 3 110-113 (1975).

14 Beavers, G.S., and Joseph, D.D. — Boundary conditions at a naturally permeable wall. J. Fluid. Mech., 30 197-207 (1967).

15 Beavers, G.S., Sparrow, E.M., and Magnuson, R.A. — Experiments on coupled parallel flows in a channel and a bounding porous medium. Stud. Appl. Maths., 50 93 (1971).

16 Rouleau, W.T. — Hydrodynamic lubrication of narrow press-fitted porous metal bearings. Trans. ASME, D 85 123-128 (1963).

17 Wu, H. — Squeeze-film behaviour for porous annular disks. Trans. ASME, F 92 593-596 (1970).

18 Wu, H. — An analysis of the squeeze film between porous rectangular plates. Trans. ASME, F 94 64-68 (1972).

19 Sparrow, E.M. Beavers, G.S., and Hwang, I.T. — Effect of velocity slip on porous walled squeeze films. Trans. ASME, F 94 260-265 (1972).

20 Wu, H. — Effect of velocity slip on the squeeze film between porous rectangular plates. Wear, 20 , 67-71 (1972).

21 Prakash, J., and Vij, S.K. — Effect of velocity slip on porous walled squeeze films. Wear, 29 363-372 (1974)

22 Murti, P.R.K. — Squeeze-film behaviour in porous circular disks. Trans. ASME, F 96 206-209 (1974).

23 Wu, H. — The squeeze film between rotating porous annular disks. Wear, 18 461-470 (1971).

24 Ting, L.L. — A mathematical analog for determination of porous annular disk squeeze film behaviour including the fluid inertia effect. Trans. ASME, D 94 417-421 (1972).

25 Cowling, T. G. — Magnetohydrodynamics. Interscience, N.Y.,(1957).

26 Elco, R.A., and Hughes, W.F. — Magnetohydrodynamic pressurization in liquid metal lubrication. Wear, 5 198 (1962).

27 Gupta, J.L., and Sinha, P. C. — Axial current induced pinch effect on the squeeze film behaviour for porous annular disks. Trans. ASME, F 97 130-133 (1975).

28 Gupta, J.L., and Patel, K. C. — Effect of axial pinch on the porous walled squeeze film with velocity slip. Wear, 31 381-389 (1975).

29 Hingu, J. V. — The effect of axial current induced pinch on the squeeze-film behaviour of porous circular disks. Wear, 40 179-184 (1976).

30 Patel, K. C. — Effect of axial current induced pinch on the squeeze film action between porous plates. Rev. Roum. Math. Pures et Appl., 22 941-949 (1977).

31 Kuzma, D.C. — Magnetohydrodynamic squeeze films. Trans. ASME, D 86, 441-444 (1964).

32 Kuzma, D.C., Maki, E.R., and Donnelly, R. J. — The magnetohydrodynamic squeeze films. J. Fluid. Mech., 19 395-400 (1964).

33 Shukla, J. B. — Hydromagnetic theory of squeeze films. Trans. ASME, D 87 142-144 (1965).

34 Sinha, P.C., and Gupta, J. L. — Hydromagnetic squeeze films between porous annular disks. J. Math. Phys. Sciences, 8 413-422 (1974).

35 Patel, K. C. — Hydromagnetic squeeze film with slip velocity between two porous annular disks. Trans. ASME, F 97 644-647 (1976).

36	Chandrasekhara, B.C.	Effect of magnetic field and velocity slip on porous walled rectangular plates. Appl. Sc. Res., 31 52-66 (1975).
37	Prakash, J., and Vij, S.K.	Hydrodynamic lubrication of a porous slider. J. Mech. Engng. Sc., 15 232-234 (1973).
38	Pinkus, O., and Sternlicht, B.	Theory of hydrodynamic lubrication. McGraw-Hill (1961).
39	Prakash, J.	Magnetohydrodynamic effects in composite bearings. Trans. ASME, F 89 323-328 (1967).
40	Agrawal, V.K.	The effect of conductivity on the load capacity of hydromagnetic composite slider bearing. Jap. J. Appl. Phys., 9 1415-1419 (1970).
41	Hughes, W.F.	The magnetohydrodynamic finite step slider bearing. Trans. ASME, D 85 129-136 (1963).
42	Cameron, A.	Basic lubrication theory. Longman (1971).
43	Murti, P.R.K.	Squeeze films in curved circular plates. Trans. ASME, F 97 650-652 (1975).

44	Kuzma, D.C.	MHD bearings Machine Design, 36 206-210 (1964).
45	Cusano, C.	Analytical investigation of an infinitely long, two-layer, porous bearing. Wear, 22 59-67 (1972).
46	Snyder, W.T.	The magnetohydrodynamic slider bearing. Trans. ASME, D 84 197-204 (1962).
47	Fucks, W., and Uhlenbusch, J.	Magnetohydrodynamic theory of lubrication. Phys. Fluids, 5 498 (1962).
48	Hughes, W. F.	The magnetohydrodynamic inclined slider bearing with a transverse magnetic field. Wear, 6 315-324 (1963).
49	Agrawal, V. K.	Inertia effects in hydromagnetic inclined slider bearing. Jap. J. Appl.Phys., 9 820-824 (1970).
50	Osterle, J.F., and Young, F.J.	On the load capacity of the hydromagnetically lubricated slider bearing. Wear, 5 227-234 (1962).
51	Agrawal, V.K.	Magnetohydrodynamiczne lozyskoslizgowe w stycznym polu magnetycznym. Rozprawy Inzynierskie, 18 47-53 (1970).
52	Kuzma, D.C.	The magnetohydrodynamic parallel plate slider bearing. Trans. ASME, D 87 778-780 (1965).

53 Ramanaiah, G. Optimum load capacity of a parallel plate slider bearing with non-uniform magnetic field. Jap. J. Appl. Phys., 6 797 (1967).

54 Prakash, J., and Vij, S.K. Effect of velocity slip on the squeeze film between rotating porous annular disks. Wear, 38 73-85 (1976).

55 Hays, D. F. Squeeze films for rectangular plates. Trans. ASME, D85, 243-246 (1963).